2014

Microemulsion-assisted synthesis of nanosized Li-Mn-O spinel cathodes for high-rate lithium-ion batteries

Xianhong Rui
Nanyang Technological University

Wenping Sun
Nanyang Technological University, wenping@uow.edu.au

QingYu Yan
Nanyang Technological University

Tuti M. Lim
Nanyang Technological University

Maria Skyllas-Kazacos
University of New South Wales

Publication Details

Rui, X., Sun, W., Yan, Q., Lim, T. Mariana. & Skyllas-Kazacos, M. (2014). Microemulsion-assisted synthesis of nanosized Li-Mn-O spinel cathodes for high-rate lithium-ion batteries. ChemPlusChem, 79 (12), 1794-1798.

Microemulsion-assisted synthesis of nanosized Li-Mn-O spinel cathodes for high-rate lithium-ion batteries

Abstract
Li1.16Mn1.84O4 nanoparticles (50-90 nm) with cubic spinel structure are synthesized by combining a microemulsion process to produce ultrafine Mn(OH)2 nanocrystals (3-8 nm) with a solid-state lithiation step. The nanostructured lithium-rich Li1.16Mn1.84O4 shows stable cycling performance and superior rate capabilities as compared with the corresponding bulk material, for example, the nano-sized Li1.16Mn1.84O4 electrode shows stable reversible capacities of 74 mAhg-1 during the 1000th cycle at a high rate of 40 C between 3.0 and 4.5 V. In addition, Li1.16Mn1.84O4 nanoparticles also show high Li storage properties over an enlarged voltage window of 2.0-4.5 V with high capacities and stable cyclability, for example, delivering discharge capacities of 209 and 114 mAhg-1 at rates of 1 and 20 C, respectively.

Keywords
assisted, microemulsion, spinel, synthesis, batteries, ion, nanosized, lithium, li, rate, mn, high, o, cathodes

Disciplines
Engineering | Physical Sciences and Mathematics

Publication Details
Rui, X., Sun, W., Yan, Q., Lim, T. Mariana. & Skyllas-Kazacos, M. (2014). Microemulsion-assisted synthesis of nanosized Li-Mn-O spinel cathodes for high-rate lithium-ion batteries. ChemPlusChem, 79 (12), 1794-1798.

ChemPubSoc Europe

DOI: 10.1002/cplu.201402267

Microemulsion-Assisted Synthesis of Nanosized Li–Mn–O Spinel Cathodes for High-Rate Lithium-Ion Batteries

Xianhong Rui,[a, b, c] Wenping Sun,[b] Qingyu Yan,*[b, c] Tuti Mariana Lim,*[d] and Maria Skyllas–Kazacos*[e]

$Li_{1.16}Mn_{1.84}O_4$ nanoparticles (50–90 nm) with cubic spinel structure are synthesized by combining a microemulsion process to produce ultrafine $Mn(OH)_2$ nanocrystals (3–8 nm) with a solid-state lithiation step. The nanostructured lithium-rich $Li_{1.16}Mn_{1.84}O_4$ shows stable cycling performance and superior rate capabilities as compared with the corresponding bulk material, for example, the nano-sized $Li_{1.16}Mn_{1.84}O_4$ electrode shows stable reversible capacities of 74 mAh g^{-1} during the 1000th cycle at a high rate of 40 C between 3.0 and 4.5 V. In addition, $Li_{1.16}Mn_{1.84}O_4$ nanoparticles also show high Li storage properties over an enlarged voltage window of 2.0–4.5 V with high capacities and stable cyclability, for example, delivering discharge capacities of 209 and 114 mAh g^{-1} at rates of 1 and 20 C, respectively.

Introduction

Spinel $LiMn_2O_4$ is one of the most attractive intercalation cathode materials for rechargeable lithium batteries owing to its natural abundance, environmental friendliness, high safety and potential high rate capability, thus making it promising for high-energy and high-power applications, such as electrical vehicles (EVs) and hybrid electrical vehicles (HEVs).[1–7] However, this material suffers from the drawback of slow dissolution of Mn^{2+} into the electrolyte according to the disproportionation reaction: $2Mn^{3+} \rightarrow Mn^{2+} + Mn^{4+}$, and thus results in a limited cycling stability. To overcome this issue, recent interests have been focused on making samples with lithium-rich compositions (e.g. $Li_{1+x}Mn_{2-x}O_4$),[3,8–12] despite compromising their theoretical capacities. The goal is to raise the valence state of manganese, which minimizes the dissolution of Mn^{2+} ions into the electrolyte and also reduces the Jahn–Teller distortion of the lattice structures.[13–15]

Meanwhile, nanostructured materials have been extensively investigated and shown enhanced power density as they can offer a range of unique advantages over their bulk counterparts including short Li^+ diffusion distance and large interfacial contact area between the electrode and electrolyte.[16–23] Among many preparation methods of nanostructures, microemulsion has been demonstrated as an effective approach to prepare nanoparticles with controllable and uniform sizes.[24–26] In this method, each water droplet acts as an independent nanoreactor to produce the desired particle with designed composition.

Herein, we show the synthesis of spinel $Li_{1.16}Mn_{1.84}O_4$ nanoparticles using a facile three-step process: 1) a microemulsion reaction to prepare ultrafine $Mn(OH)_2$ nanoparticles, 2) the $Mn(OH)_2$ nanoparticles decompose to Mn_3O_4, and 3) a solid state reaction between Mn_3O_4 and Li_2CO_3 to form $Li_{1.16}Mn_{1.84}O_4$. When evaluated as a cathode material for lithium-ion batteries, the spinel $Li_{1.1}Mn_{1.9}O_4$ nanoparticles exhibited a stable cycling performance and superior rate capability, for example, delivering reversible capacities of 74 (at 40 C) and 114 mAh g^{-1} (at 20 C) in the voltage ranges of 3.0–4.5 V and 2.0–4.5 V, respectively.

Results and Discussion

As shown in Figure 1a, the X-ray powder diffraction (XRD) pattern of the precursors obtained by the microemulsion reaction of $MnCl_2$ and ammonia indicates that they are $Mn(OH)_2$ (JCPDS No. 12-0696). A broad hump at 2θ of about 30° is attributed to the signal from the glass holder.

[a] Dr. X. Rui[+]
School of Energy and Environment
Anhui University of Technology
Maanshan, Anhui 243002 (P. R. China)

[b] Dr. X. Rui,[+] Dr. W. Sun,[+] Prof. Q. Yan
School of Materials Science and Engineering
Nanyang Technological University
Singapore 639798 (Singapore)
Fax: (+65) 67909081
E-mail: alexyan@ntu.edu.sg

[c] Dr. X. Rui,[+] Prof. Q. Yan
Energy Research Institute
Nanyang Technological University
Singapore 637459 (Singapore)

[d] Dr. T. M. Lim
School of Civil and Environmental Engineering
Nanyang Technological University
Singapore 639798 (Singapore)
Fax: (+65) 67910676
E-mail: tmlim@ntu.edu.sg

[e] Prof. M. Skyllas–Kazacos
School of Chemical Engineering
The University of New South Wales
Sydney NSW 2052 (Australia)
Fax: (+61) (2) 93855966
E-mail: m.kazacos@unsw.edu.au

[+] These authors contributed equally to this work.

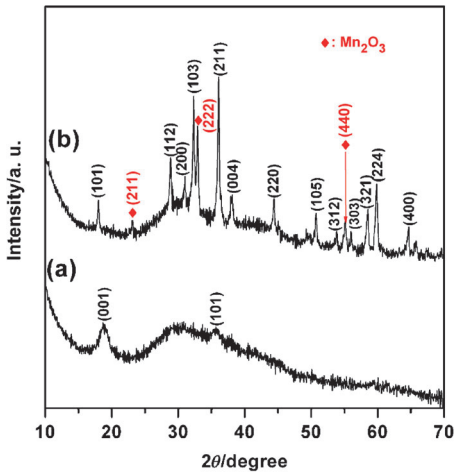

Figure 1. XRD patterns of the precursors prepared by microemulsion reaction (a) and the intermediates obtained by heating the precursors at 600 °C for 2 h (b).

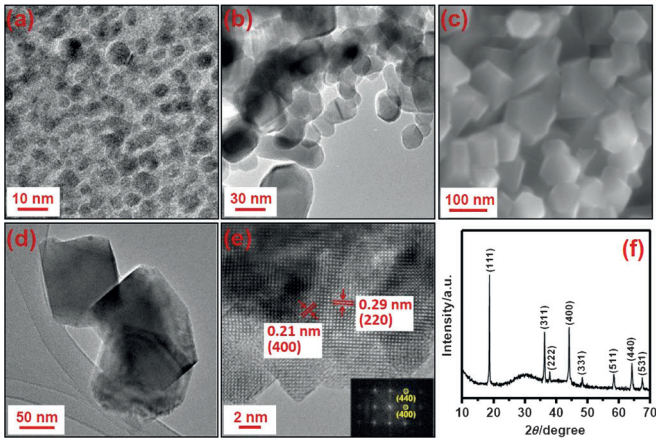

Figure 2. a) TEM image of the precursors prepared by microemulsion reaction. b) TEM image of the intermediates obtained by heating the precursors at 600 °C for 2 h. c) FESEM, d) TEM, e) HRTEM images and f) XRD pattern of final $Li_{1.16}Mn_{1.84}O_4$ products. Inset in (e): the FFT pattern of Figure 2e.

The transmission electron microscopy (TEM) image (Figure 2a) shows that the $Mn(OH)_2$ consisted of spherical particles with sizes of 3–8 nm. Heating $Mn(OH)_2$ in air at 600 °C for 2 h, as indicated by the XRD pattern in Figure 1b, except for the diffraction peaks of Mn_3O_4 (JCPDS No. 24-0734), some impurities of Mn_2O_3 (JCPDS No. 76-0150) are observed. Meanwhile, the particle size is increased to 10–50 nm as confirmed by the TEM image (Figure 2b). Subsequently, the Mn_3O_4 nanoparticles went through a lithiation process by treating with Li_2CO_3. The field-emission scanning electron microscopy (FESEM) and TEM images (Figure 2c,d) show that the resulting samples are nanoparticles with sizes of 50–90 nm. The inductively coupled plasma (ICP) analysis reveals that the composition of the sample after the lithiation process is $Li_{1.16}Mn_{1.84}O_4$. While the corresponding XRD pattern (Figure 2f) shows the signature peaks of the cubic spinel structure (space group: *Fd3m*, JCPDS No. 35-0782). Moreover, the average grain size *D* is calculated to be around 55 nm using the Scherrer's equation on the basis of reflection peaks of (111), (400) and (311), which is consistent with the TEM observation. The high-resolution (HR) TEM image of an individual $Li_{1.16}Mn_{1.84}O_4$ nanoparticle (Figure 2e) and the corresponding fast Fourier transform (FFT) analysis (inset in Figure 2e) suggest the nature of single-crystalline material. The lattice fringes with spacing of 0.21 and 0.29 nm are indexed to the (400) and (220) planes of spinel $Li_{1.16}Mn_{1.84}O_4$, respectively.

As a comparison, we also prepared samples by direct precipitation of $Mn(OH)_2$ in water without formation of a microemulsion followed by heating in air and the lithiation processes. The XRD pattern (Figure 3a) indicates that the resulting

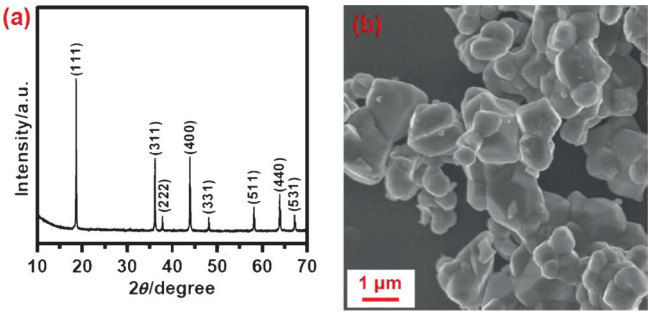

Figure 3. a) XRD pattern and b) FESEM image of the sample prepared without using the microemulsion process.

sample also has a cubic spinel structure (space group: *Fd3m*, JCPDS No. 35-0782), meanwhile the ICP measurement confirms the sample composition is close to $Li_{1.16}Mn_{1.84}O_4$. The FESEM image (Figure 3b) shows that the products are large particles with sizes in the range of 0.5–2 μm, which is noted as bulk $Li_{1.16}Mn_{1.84}O_4$.

To study the cathode performance of $Li_{1.16}Mn_{1.84}O_4$, a series of electrochemical measurements were carried out based on the half-cell configuration.[27–30] Figure 4a shows the initial charge–discharge voltage profiles of bulk and nano-sized $Li_{1.16}Mn_{1.84}O_4$ electrodes at a rate of 0.5 C between 3.0 and 4.5 V. Both the charge and discharge curves exhibit two plateaus at approximately 4.0 and 4.1 V, which represent the typical electrochemical feature of spinel $LiMn_2O_4$.[31] The nano-sized electrode depicts an initial charge capacity of 126 mAh g^{-1} and a subsequent discharge capacity of 110 mAh g^{-1}, giving a Coulombic efficiency of 87%. Thereafter, the Coulombic efficiency is gradually close to 100% upon progressive cycling and the discharge capacity can be stabilized at 105 mAh g^{-1} during the 100th cycle, showing that the capacity retention is as high as 96% (Figure 4b). The bulk $Li_{1.16}Mn_{1.84}O_4$ electrode exhibits inferior cyclability (Figure 4b), which decreases from 108 mAh g^{-1} for the first cycle to 86 mAh g^{-1} for the 100th cycle with a capacity retention of only 80%. To further investigate the application in high power density devices, the cells were discharged at different rates ranging from 1 C to 60 C with a charging rate of 1 C (Figure 4c). The nano-sized $Li_{1.16}Mn_{1.84}O_4$ cathode shows discharge capacities of 105, 100, 96, 89, 85 and 81 mAh g^{-1} during the 2nd cycle at rates of 1, 5, 10, 20, 30 and 40 C, respectively. Remarkably, even at a high rate of 60 C, it can still

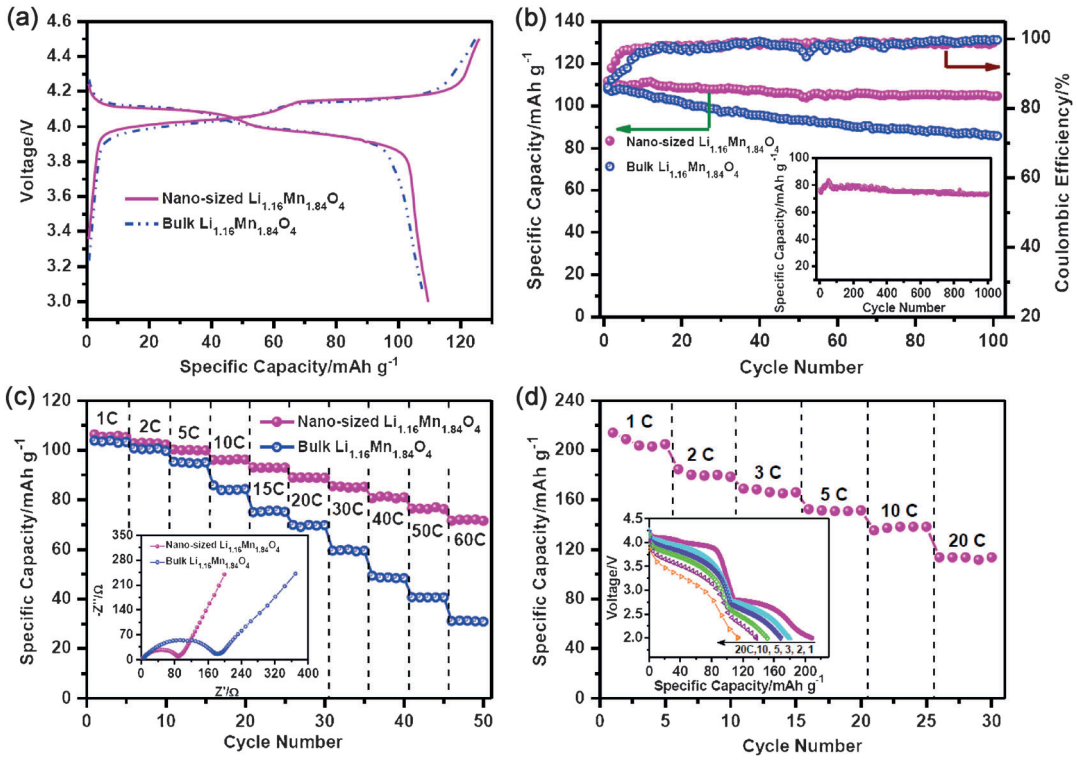

Figure 4. Electrochemical characterization of bulk and nano-sized $Li_{1.16}Mn_{1.84}O_4$. a) Initial charge–discharge profiles and b) cycling performance of two electrodes at a rate of 0.5 C between 3.0 and 4.5 V. In this voltage window, 1 C = 130 mA g^{-1}. Inset in (b): long-term cycling performance of nano-sized $Li_{1.16}Mn_{1.84}O_4$ electrode at a high rate of 40 C. c) A comparison of discharge capacities of two electrodes at various current rates of 1 to 60 C. Inset in (c): corresponding electrochemical impedance spectra. d) The rate capability of nano-sized $Li_{1.16}Mn_{1.84}O_4$ electrode in an enlarged voltage window of 2.0–4.5 V. Inset in (d): representative discharge curves at various rates. Here, 1 C = 296 mA g^{-1}.

deliver a discharge capacity of 72 mAh g^{-1} during the 2nd cycle. Such high-C-rate performance is far better than that of the bulk material, which only depicts low discharge capacities of 49 and 31 mAh g^{-1} at 40 C and 60 C, respectively (Figure 4c). The inferior Li storage property of bulk $Li_{1.16}Mn_{1.84}O_4$ is mainly attributed to its slow kinetics of Li diffusion and electron transport. The electrochemical impedance spectrum (inset in Figure 4c) of the bulk $Li_{1.16}Mn_{1.84}O_4$ cathode shows a larger radius of semicircle in the Nyquist plots as compared to that of the nano-sized $Li_{1.16}Mn_{1.84}O_4$ cathode, which indicates a larger charge-transfer resistance. Moreover, the nano-sized $Li_{1.16}Mn_{1.84}O_4$ cathode exhibits an excellent cyclability at a high rate of 40 C (inset in Figure 4b), delivering a discharge capacity of 74 mAh g^{-1} during the 1000th cycle. As compared to ever-reported Li–Mn–O spinel cathodes,[3,32–34] for example, 72 mAh g^{-1} for mesoporous $Li_{1.12}Mn_{1.88}O_4$ at 3000 mA g^{-1} (23 C)[3] and 76 mAh g^{-1} for porous $LiMn_2O_4$ microspheres at 20 C (decreasing to 47 mAh g^{-1} after 1000 cycles),[32] the above performance of nano-sized $Li_{1.16}Mn_{1.84}O_4$ electrode is also excellent.

It is known that Li^+ can be intercalated in the empty octahedral sites of the $LiMn_2O_4$ spinel structure at around 3.0 V to form $Li_{1+x}Mn_2O_4$.[35] However, the material suffers from a drastic capacity loss because of the difficulty in the reversible phase transition between the cubic $LiMn_2O_4$ and the tetragonal $Li_2Mn_2O_4$ structure. Thus, we also evaluated the cycling responses of nano-sized $Li_{1.16}Mn_{1.84}O_4$ electrode at different C rates in the voltage rang of 2.0–4.5 V (Figure 4d). The electrode shows second-cycle discharge capacities of 209, 180, 169, 152, 137 and 114 mAh g^{-1} at rates of 1, 2, 3, 5, 10 and 20 C, respectively. With the increased current density, the plateaus in the voltage profile move downward (inset in Figure 4d) owing to increased overpotentials of the electrode and the internal *IR* drop.[31] Although the electrode undergoes fast structural change from cubic to tetragonal phase, it exhibits high discharge capacities with good reversibility.

The above demonstrated high-performance nano-sized $Li_{1.16}Mn_{1.84}O_4$ cathode is believed to result from its beneficially morphological and structural features. The nanodimensional particles (50–90 nm) offer a large contact area with the electrolyte and short diffusion distances for lithium-ion intercalation/deintercalation, leading to a high power performance. Furthermore, the lithium-rich compound (i.e., $Li_{1.16}Mn_{1.84}O_4$) raises the valence state of manganese, which can alleviate the dissolution of Mn^{2+} ions into the electrolyte through disproportionation reaction and reduce the Jahn–Teller distortion, resulting in significantly enhanced cycling stability.

Conclusion

A microemulsion-assisted synthetic approach has been developed to prepare lithium-rich spinel $Li_{1.16}Mn_{1.84}O_4$ nanoparticles. The sample shows excellent Li storage properties at high current densities. The nano-sized $Li_{1.16}Mn_{1.84}O_4$ cathode also exhib-

its highly reversible specific capacities in the large voltage window, which involves the phase transition between the cubic and tetragonal phase. For example, when discharged at a high rate of 40 C in the voltage range of 3.0–4.5 V, the electrode exhibits stable capacities of 74 mAh g^{-1} during the 1000th cycle. In the enlarged voltage window of 2.0–4.5 V, the electrode is still able to deliver a high discharge capacity of 114 mAh g^{-1} at 20 C with good cyclability.

Experimental Section

In a typical procedure, $C_{16}H_{33}(OCH_2CH_2)_{10}OH$ (brij 56; 5 g) was dissolved in iso-octane (30 mL) by ultrasonication to obtain a transparent solution. Successively, $MnCl_2$ (0.2 mM) was dissolved in 0.1 M HCl solution (100 μL) and added into the iso-octane solution under ultrasonication. After 30 min, of ammonia (25 wt%, 300 μL) was added to above mixture. The reaction was stirred at 35 °C for 1 h and subsequently washed with *n*-hexane and ethanol several time and dried at 70 °C. This procedure resulted in ultrafine $Mn(OH)_2$ nanoparticles with a yield of approximately 15 mg. More $Mn(OH)_2$ (~100 mg) was obtained by repeating the above process several times. Then, Mn_3O_4 (≈85 mg) was prepared by heating $Mn(OH)_2$ (≈100 mg) at 600 °C for 2 h under a heating rate of 5 °C min^{-1} in air. Thereafter, Mn_3O_4 (≈85 mg) was mixed with Li_2CO_3 (≈27 mg) at a molar ratio of 1:1 by energetically grinding with a mortar and pestle for 2 h, and calcined at 800 °C for 6 h under a heating rate of 5 °C min^{-1} in air. After the calcination, the resulting material was washed with water and then dried at 70 °C. The overall synthetic procedure is illustrated in Scheme 1.

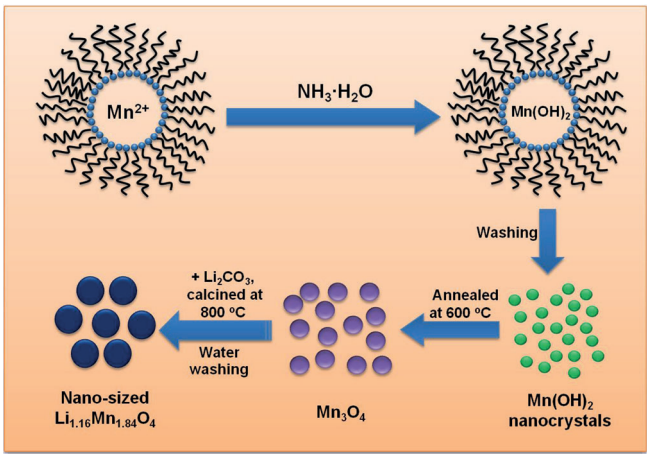

Scheme 1. Schematic of microemulsion-assisted preparation of $Li_{1.16}Mn_{1.84}O_4$ nanoparticles.

X-ray powder diffraction (XRD) patterns were recorded on a Bruker AXS D8 advance X-ray diffractometer at the 2θ range of 10 to 70° using CuKα radiation. The morphology was investigated by a field-emission scanning electron microscopy (FESEM) system (JEOL, Model JSM-7600F), and the nanostructure was characterized by a transmission electron microscopy (TEM) instrument (JEOL, Model JEM-2010) operating at 200 kV. Inductively coupled plasma (ICP, Dual-view Optima 5300 DV ICP-OES system) was employed to measure the elemental contents of lithium and manganese.

The cathodes were fabricated by mixing $Li_{1.16}Mn_{1.84}O_4$, multiwalled carbon nanotubes and poly(vinyldifluoride) at a weight ratio of 80:10:10 in *n*-methyl-2-pyrrolidone solvent. Lithium foil was used as the anodes and the electrolyte solution was made of 1 M $LiPF_6$ in ethylene carbonate (EC)/dimethyl carbonate (1/1, w/w). The cells were tested on a NEWARE multichannel battery test system with galvanostatic charge and discharge in the voltage ranges of 3.0–4.5 and 2.0–4.5 V.

Acknowledgement

*We gratefully acknowledge, NRF2009EWT-CERP001-026 (Singapore), A*STAR SERC (grant 1021700144), Singapore MPA 23/04.15.03 grant and Singapore National Research Foundation under CREATE program: EMobility in Megacities.*

Keywords: cathodes · high-rate capability · lithium manganese oxide · microemulsions · nanoparticles

[1] J. M. Tarascon, E. Wang, F. K. Shokoohi, W. R. McKinnon, S. Colson, *J. Electrochem. Soc.* **1991**, *138*, 2859–2864.
[2] A. R. Armstrong, P. G. Bruce, *Nature* **1996**, *381*, 499–500.
[3] F. Jiao, J. L. Bao, A. H. Hill, P. G. Bruce, *Angew. Chem. Int. Ed.* **2008**, *47*, 9711–9716; *Angew. Chem.* **2008**, *120*, 9857–9862.
[4] S. Lim, J. Cho, *Electrochem. Commun.* **2008**, *10*, 1478–1481.
[5] X. Rui, Q. Yan, M. Skyllas-Kazacos, T. M. Lim, *J. Power Sources* **2014**, *258*, 19–38.
[6] X. Rui, X. Zhao, Z. Lu, H. Tan, D. Sim, H. H. Hng, R. Yazami, T. M. Lim, Q. Yan, *ACS Nano* **2013**, *7*, 5637–5646.
[7] X. Rui, H. Tan, Q. Yan, *Nanoscale* **2014**, *6*, 9889–9924.
[8] Z. H. Chen, K. Amine, *J. Electrochem. Soc.* **2006**, *153*, A1279–A1283.
[9] B. J. Liddle, S. M. Collins, B. M. Bartlett, *Energy Environ. Sci.* **2010**, *3*, 1339–1346.
[10] Z. Li, N. A. Chernova, J. J. Feng, S. Upreti, F. Omenya, M. S. Whittingham, *J. Electrochem. Soc.* **2012**, *159*, A116–A120.
[11] Z. Lu, X. Rui, H. Tan, W. Zhang, H. H. Hng, Q. Yan, *ChemPlusChem* **2013**, *78*, 218–221.
[12] J. Liu, W. Liu, S. Ji, Y. Zhou, P. Hodgson, Y. Li, *ChemPlusChem* **2013**, *78*, 636–641.
[13] M. S. Whittingham, *Chem. Rev.* **2004**, *104*, 4271–4301.
[14] Q. Liu, S. Wang, H. Tan, Z. Yang, J. Zeng, *Energies* **2013**, *6*, 1718–1730.
[15] M. S. Islam, C. A. J. Fisher, *Chem. Soc. Rev.* **2014**, *43*, 185–204.
[16] X. H. Rui, J. X. Zhu, W. L. Liu, H. T. Tan, D. H. Sim, C. Xu, H. Zhang, J. Ma, H. H. Hng, T. M. Lim, Q. Y. Yan, *RSC Adv.* **2011**, *1*, 117–122.
[17] X. H. Rui, J. X. Zhu, D. Sim, C. Xu, Y. Zeng, H. H. Hng, T. M. Lim, Q. Y. Yan, *Nanoscale* **2011**, *3*, 4752–4758.
[18] X. H. Rui, D. H. Sim, C. Xu, W. L. Liu, H. T. Tan, K. M. Wong, H. H. Hng, T. M. Lim, Q. Y. Yan, *RSC Adv.* **2012**, *2*, 1174–1180.
[19] Y. Yang, D. Kim, P. Schmuki, *Electrochem. Commun.* **2011**, *13*, 1198–1201.
[20] L. Wang, L. C. Zhang, I. Lieberwirth, H. W. Xu, C. H. Chen, *Electrochem. Commun.* **2010**, *12*, 52–55.
[21] X. Rui, Z. Lu, Z. Yin, D. H. Sim, N. Xiao, T. M. Lim, H. H. Hng, H. Zhang, Q. Yan, *Small* **2013**, *9*, 716–721.
[22] K. Zhu, X. Yan, Y. Zhang, Y. Wang, A. Su, X. Bie, D. Zhang, F. Du, C. Wang, G. Chen, Y. Wie, *ChemPlusChem* **2014**, *79*, 447–453.
[23] D. Chen, H. Quan, G.-S. Wang, L. Guo, *ChemPlusChem* **2013**, *78*, 843–851.
[24] Q. Y. Yan, A. Purkayastha, T. Kim, R. Kroger, A. Bose, G. Ramanath, *Adv. Mater.* **2006**, *18*, 2569–2573.
[25] Y. Wang, H. Rong, B. Li, L. Xing, X. Li, W. Li, *J. Power Sources* **2014**, *246*, 213–218.
[26] S. Xu, S. Zhang, J. Zhang, T. Tan, Y. Liu, *J. Mater. Chem. A* **2014**, *2*, 7221–7228.
[27] D. Hao Sim, X. H. Rui, J. Chen, H. T. Tan, T. M. Lim, R. Yazami, H. H. Hng, Q. Y. Yan, *RSC Adv.* **2012**, *2*, 3630–3633.

[28] C. M. Zhang, J. Chen, Y. Zeng, X. H. Rui, J. X. Zhu, W. Y. Zhang, C. Xu, T. M. Lim, H. H. Hng, Q. Y. Yan, *Nanoscale* **2012**, *4*, 3718 – 3724.
[29] X. H. Rui, C. Li, J. Liu, T. Cheng, C. H. Chen, *Electrochim. Acta* **2010**, *55*, 6761 – 6767.
[30] X. H. Rui, C. Li, C. H. Chen, *Electrochim. Acta* **2009**, *54*, 3374 – 3380.
[31] H. W. Lee, P. Muralidharan, R. Ruffo, C. M. Mari, Y. Cui, D. K. Kim, *Nano Lett.* **2010**, *10*, 3852 – 3856.
[32] L. J. Xi, H. E. Wang, Z. G. Lu, S. L. Yang, R. G. Ma, J. Q. Deng, C. Y. Chung, *J. Power Sources* **2012**, *198*, 251 – 257.
[33] F. Y. Cheng, H. B. Wang, Z. Q. Zhu, Y. Wang, T. R. Zhang, Z. L. Tao, J. Chen, *Energy Environ. Sci.* **2011**, *4*, 3668 – 3675.
[34] H. X. Liang, X. Zhao, Z. Y. Yu, M. H. Cao, H. X. Liu, *Solid State Ionics* **2011**, *192*, 339 – 342.
[35] T. Ohzuku, M. Kitagawa, T. Hirai, *J. Electrochem. Soc.* **1990**, *137*, 769 – 775.

Received: August 18, 2014
Revised: October 10, 2014
Published online on October 27, 2014